Semiconductor Physics, Quantum Electronics & Optoelectronics, 2026. V. 29, No 1. P. 105-117.

Optoelectronics and optoelectronic devices

Enhanced photovoltaic performance and minimal hysteresis of perovskite solar cells using caffeine-modified $MAPbI_3$ light-harvesting material

M.I. Amanyi[1], E. Danladi[1,2*], A.O. Salawu[3], A.I. Alhaji[4], K.A. Ogunmoye[5], O.E. Onah[1], M.T. Ekwu[6]

[1]*Department of Physics, Federal University of Health Sciences, Otukpo, Benue State, Nigeria*
[2]*Department of Mathematical and Physical Sciences, Central University of Technology, Free State, South Africa*
[3]*Department of Computer Science, Nile University of Nigeria*
[4]*Department of Science Education, Federal University, Dutsin-Ma, Katsina State, Nigeria*
[5]*Department of Physics and Astronomy, Appalachian State University, Boone, North Carolina, USA*
[6]*Department of Physics, Air Force Institute of Technology, Kaduna, Nigeria*
[*]*Corresponding author e-mail: danladielibako@gmail.com*

Abstract. Perovskite solar cells (PSCs) have become a rising star in the horizon of photovoltaics due to their cost-effectiveness and simple fabrication process. Despite their prospects, the viability of their commercialization has been hampered due to low power conversion efficiency (PCE) and hysteresis. In this paper, caffeine was incorporated into methylammonium lead iodide ($MAPbI_3$) with different wt% (0.5, 1.0, and 1.5 wt%) to fabricate perovskite solar cell devices. The effects of caffeine inclusion were probed to uncover its influence on enhancing light absorption, improving crystallinity, boosting the device performance, and mitigating the disparity in current-voltage measurement (hysteresis). The presence of caffeine results in improved absorption, diminished band gap, and improved film crystallinity. Perovskite solar cells with caffeine molecules demonstrated improved metric parameters (PCE, fill factor FF, short-circuit current density J_{sc}, and open-circuit voltage V_{oc}) compared to a pure device without caffeine. Particularly, the device with 1.0 wt% caffeine in $MAPbI_3$ shows the best performance with PCE of 14.072%, FF of 0.640, J_{sc} of 23.083 mA/cm^2, and V_{oc} of 0.953 V. The disparity in current-voltage measurement for all caffeine-based devices was reduced. Specifically for the device with 1.0 wt% of caffeine, the hysteresis index is 0.0300. The device without caffeine shows PCE = 6.157%, FF = 63.9%, J_{sc} = 10.132 mA/cm^2, and V_{oc} = 0.951 V, and performs worse than all caffeine-based devices. The enhanced device performance observed in the caffeine-modified perovskite is primarily attributed to reduced series resistance and concentration of non-radiative recombination centers, leading to more efficient charge transport and increased carrier lifetime within the absorber layer.

Keywords: perovskite solar cells, caffeine, hysteresis, $MAPbI_3$, photovoltaics.

https://doi.org/10.15407/spqeo29.01.105
PACS 41.20.Cv, 61.43.Bn, 68.55.ag, 68.55.jd, 72.80.Tm, 73.25.+i

Manuscript received 10.06.25; revised version received 02.03.26; accepted for publication 18.03.26; published online 25.03.26.

1. Introduction

The issue of energy can be considered as a necessity and a fundamental problem facing the world today due to the increase in population growth and advancement in technological deployment. At present, the demand for energy is satisfied by over 80% of fossil fuels [1, 2]. However, due to the large depletion of crude reserves and unfavorable environmental effects caused by combustion, alternative energy sources are now receiving a lot of attention [3, 4]. In this case, photovoltaic (PV) industrialists and researchers have developed solar technology instead of traditional non-renewable energy sources.

Greater efforts are needed to eliminate carbon footprints while meeting energy needs and addressing the challenges of global warming. Dependence on hydrocarbons can be reduced by solar energy using effective and non-toxic methods [5, 6].

Solar energy has the potential to meet the world rising energy needs, but doing so will require ongoing scientific research to make solar energy both affordable and efficient. Researchers are currently looking for new types of solar cells employing diverse concepts, materials, and designs [7, 8].

Organic-inorganic perovskite materials are at the forefront in research due to their distinctive optical and

electronic properties, namely, high coefficient of absorption, effective carrier transport properties, small exciton binding energy, elongated carrier lifetime, high dielectric constant, and an appropriate bandgap that can find application in several devices [9–13]. Perovskite materials have demonstrated rapid progress and have been used with promising outcomes [14]. The efficiency of PSCs has progressed greatly from 3.8% to > 25% in just a few years [5, 15, 16]. Despite the outstanding progress in efficiency, the commercialization of PSCs is still hindered by long-term stability and hysteresis, which is attributed to discrepancies in current-voltage measurements [17, 18].

Yang *et al.* [19] enhanced the PCE of PSC using an iodine confining strategy by incorporating poly(2-vinylpyridine) (P2VP) into the perovskite film. P2VP effectively bonds with iodine species from perovskite decomposition to inhibit its diffusion and volatilization from PSCs, thus suppressing perovskite decomposition and device degradation while maintaining 90.9% of its initial efficiency after 85 °C for 750 h. Seo and co-workers used a fluorene-terminated HTM to achieve 500 h of stable efficiency at 85 °C in air [20]. Abdi-Jalebi *et al.* [21] have shown that losses due to non-radiative recombination and photo-induced ion migration in the perovskite film interface could be controlled substantially through passivation of the surface and give rise to fewer grain boundaries. Jin *et al.* [22] have demonstrated that the addition of KSCN can give improved crystal film through crystallization growth, decrease the grain boundaries while increasing the grain size, reduce the trap sites, decrease instability, increase mobility of carriers, and minimize differences in hysteresis effect, resulting in high-quality film. Grätzel and co-workers incorporated PMMA in anti-solvent as a template for film growth control to produce a perovskite film with minimal surface defects [23, 24]. In another study by Guo *et al.*, where new types of non-fullerene small molecules were added during anti-solvent treatment to passivate surface defects corresponding to Pb^{2+}, the obtained device demonstrated efficiency exceeding 18% in a *p-i-n* configuration [25]. Also, Yang *et al.* documented the modulation of I_2 for anti-solvent treatment that gave a highly crystalline $MAPbI_3$ characterized by a minor surface defect concentration and less instability [26]. Molecules with semiconducting properties in Lewis acid or base, having carbonyl or cyano functions in anti-solvent for passivation of surface traps, were utilized by Niu *et al.* [27]. A fabricated high-quality $CH_3NH_3PbI_3$ film through the addition of Hydrogen Iodide (HI) into chlorobenzene produces enhanced phase purity and chemical homogeneity, resulting in improved PCE of 19.9% from 17.3% with improved stability [19]. Thus, it can be affirmed that the presence of additives in anti-solvents can serve as a potential route to enhance PSCs. From previous research, good additives used in PSC should have the following features: (i) good conductivity, (ii) comparable annealing temperature, (iii) exceptional bonding ability for passivating defects, and (iv) good hydrophobicity to environmental stability enhancement.

Caffeine is a planar, and conjugated aromatic compound made up of 10π electrons. As a result, caffeine has the potential to simultaneously function as a passivating material on $MAPbI_3$ and also transport charges within a short distance. Therefore, caffeine, made of lone pair atoms of nitrogen in a small molecule, is a conjugated polymer and has the potential of acting as a stimulating additive in PSCs [28–31].

This work aims to develop high-quality perovskite films by employing caffeine as an additive to create a strong interaction with Pb^{2+} ions to slow down the perovskite crystal growth and boost the performance of the perovskite solar cell.

2. Materials and methods

2.1. Materials

Fluorine doped tin oxide (FTO) coated glass (SOLARONIX, 15 Ω/sq), titanium isopropoxide (SIGMA-ALDRICH), acetic acid (CH_3COOH), methylamine solution (CH_3NH_2), and lead iodide (PbI_2) were obtained from TCI Inc, caffeine, toluene, and distilled water were obtained from BDH chemicals, ethanol was obtained from sigma Aldrich, MAI was obtained from BDH chemicals. All the chemicals were used without further purification.

2.2. Preparation of $MAPbI_3$ and caffeine modified $MAPbI_3$ films

The $MAPbI_3$ and caffeine-modified $MAPbI_3$ absorbing films were prepared following the procedure: a certain amount of caffeine (7.8 g) was dissolved in 20 mL of dimethyl formamide and sonicated for 1 min to form a uniformly dispersed caffeine solution. In a 3:1 molar ratio of MAI and PbI_2, caffeine in different amounts (0.5, 1.0, and 1.5 wt%) was added into the mixture and stirred for 30 min to ensure uniform distribution of films.

2.3. Preparation of photoanode

The photoanode was prepared by first cleaning the FTO using sodium laureth sulphate. The compact titanium (c-TiO_2) was spin-coated dynamically on FTO at 4000 rpm for 20 s. The film was dried at 120 °C for 10 min, and it was then annealed for 30 min at 450 °C. m-TiO_2 (mesoporous) was deposited on c-TiO_2 using spin coating at 4000 rpm for 20 s. The pristine $MAPbI_3$ and caffeine-modified $MAPbI_3$ were then spin-coated at 4000 rpm for 20 s on top of m-TiO_2. The as-deposited pristine $MAPbI_3$ and caffeine-modified $MAPbI_3$ perovskite films were annealed at 110 °C for 1 h. The hole transport layer was CuI, which was deposited using spin coating and annealed at 150 °C.

2.4. Assembly of the cells

The photoanodes of 4 cells and the counter electrodes made of Elcocarb were sealed with ethylene-vinyl acetate to form 4 PSCs. The schematic of PSC is shown in Fig. 1.

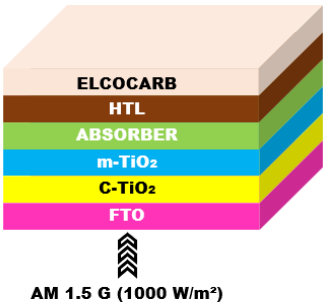

Fig. 1. Schematic diagram of the fabricated PSC.

2.5. Characterization and measurement

UV-vis spectroscopy was performed using an Axiom Medicals (UV752 UV-Vis-NIR) spectrophotometer. The crystal phase identification of the film was performed using an X-ray diffractometer (Rigaku D, Max 2500) with $CuK_{\alpha 1}$ radiation, $\lambda = 1.5406$ Å, and 2θ scanning angle ranging from 10 to 80° at 300 K. The morphologies of the films were obtained using Scanning Electron Microscopy JEOL (JSM-7600F) operated at a voltage of 20 kV. The photovoltaic performance of the fabricated devices was evaluated using a setup made of a Xenon lamp and a filter coupled to a Keithley-2400 source meter at the 100 mW/cm^2 illumination irradiance.

3. Results and discussion

3.1. Optical properties

3.1.1. Optical absorbance, transmittance, reflectance, and refractive index

The UV-vis absorption spectra of pure $MAPbI_3$, 0.5, 1.0, and 1.5 wt% of caffeine are depicted in Fig. 2a, while the corresponding transmittance spectra are shown in Fig. 2b. Fig. 2c represents the reflectance properties of pure $MAPbI_3$, 0.5, 1.0, and 1.5 wt% of caffeine, while Fig. 2d shows the optical refractive index of the studied samples. It can be seen that the pure $MAPbI_3$ and all the samples with caffeine demonstrated strong optical absorption bands in the visible region, due to an indirect transition [32], which agrees with similar studies [33, 34]. The absorption spectra exhibit a strong and broad absorption between 400…800 nm, with a sharp edge close to 770…800 nm, corresponding to the direct bandgap of $MAPbI_3$. The high absorption coefficient in this region is caused by direct interband electronic transitions from the valence band (I 5p orbitals) to the conduction band (Pb 6p orbitals) [5]. With increasing the caffeine concentration (0.5…1.5 wt%), the absorbance intensity is noticeably enhanced in the visible range. This improvement suggests better film quality, enhanced crystallinity, and reduced defect density, which promote stronger light–matter interaction and more efficient photon harvesting. The absence of a significant shift in the absorption edge indicates that caffeine primarily influences structural and defect properties rather than altering the intrinsic bandgap of $MAPbI_3$.

Pure $MAPbI_3$ and all the samples with caffeine showed a high transparency in the visible region with a corresponding peak and a valley in the infrared region. The transmittance is stronger in the pure $MAPbI_3$ sample, which means that surface defects and crystal size are the primary reasons for the observed variations in the film transmittance.

The optical reflectance increases with increasing wavelength in the visible region. This observation is due to an increase in the absorption shown in Fig. 2a. The refractive index (n) is a crucial parameter, because a lot of optical properties are affected by this parameter [35]. The refractive index of an optical material has a relationship with its ion electronic polarization and the local field inside it [36]. The formula used in obtaining the refractive index is shown in Eq. (1) [35]:

$$n = \frac{1+\sqrt{R}}{1-\sqrt{R}}, \tag{1}$$

where R is the optical reflectance.

3.1.2. Absorption and extinction coefficient

Fig. 3a depicts an absorption coefficient α of the pure $MAPbI_3$ and all samples with caffeine. α of a material defines the measure of penetration that light can travel before being absorbed [37]. The value of α increased with increasing the caffeine content from 0.5 to 1.0 wt% and decreased drastically at 1.5 wt% of caffeine. This increase can be attributed to the modulating ability of caffeine in enhancing the quality of the perovskite crystal. The enhanced crystallinity results in fewer defects and traps in the crystal structure. However, an excessive addition of caffeine beyond 1.0 wt% results in non-uniform crystal growth, giving rise to smaller, disordered grains, which reduces the material's ability to absorb light efficiently.

Fig. 3b shows the extinction coefficient k as a function of photon energy for the studied samples. k follows a similar pattern of behavior as the absorption coefficient. The sudden increase is attributed to the caffeine interaction with the perovskite precursors, resulting in improved crystallinity of the film. This improved crystallinity usually results in better alignment of the crystal planes and fewer grain boundaries, which can enhance the material interaction with light, thus increasing the extinction coefficient.

3.1.3. Optical and opto-electrical conductivity

The optical conductivity, σ_{opt}, of a film is the property of a material that describes how such films respond to light [5]. This parameter is highly indispensable in understanding how materials interact with photons. σ_{opt} was obtained using Eq. (2), where c stands for light speed, and the refractive index is denoted as n [35]:

$$\sigma_{opt} = \frac{\alpha n c}{4\pi}. \tag{2}$$

Fig. 4a shows the optical conductivity dependence on photon energy. The optical conductivity decreases with lower photon energy (*i.e.*, longer wavelength). The optical conductivity increased with increasing the caffeine content in $MAPbI_3$ from 0.5 to 1.0 wt% before it

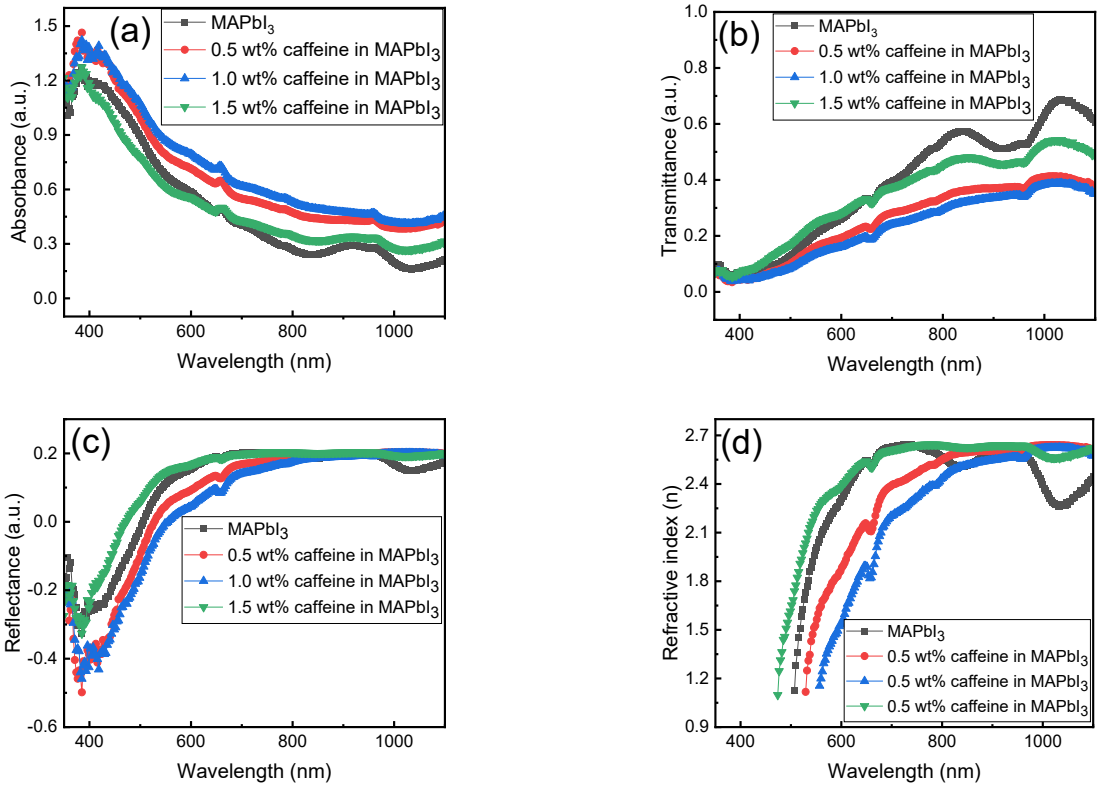

Fig. 2. Optical absorbance (a), transmittance (b), reflectance (c), and refractive index (d) with wavelength.

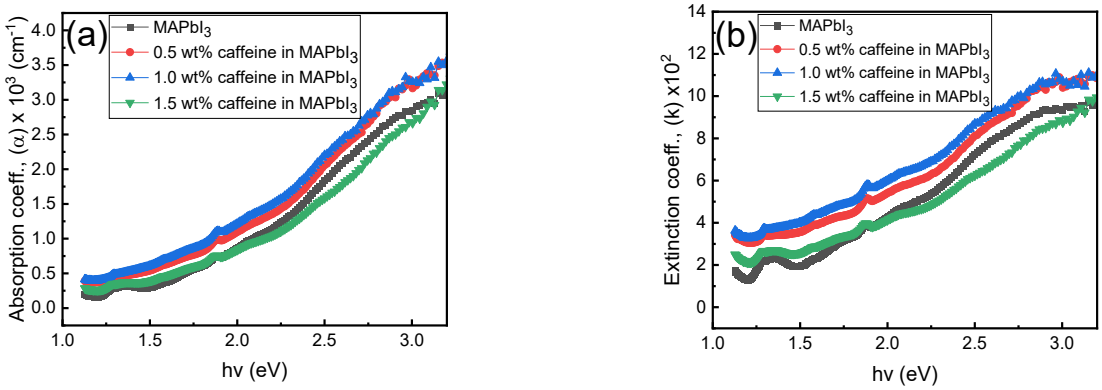

Fig. 3. Absorption (a) and extinction (b) coefficients with photon energy for pure $MAPbI_3$ and samples with caffeine.

decreased thereafter. This increase in conductivity is attributed to an improvement in the arrangement of atoms or molecules in the $MAPbI_3$ film, creating pathways for easier charge carrier movement. This enhanced mobility results in better response to light, thus increasing the optical conductivity.

The opto-electrical conductivity σ_{elec} of the films was calculated from Eq. (3) [35]:

$$\sigma_{elec} = \frac{2\lambda\sigma_{opt}}{\alpha}, \quad (3)$$

where α stands for the absorption coefficient, and λ represents the wavelength.

The opto-electrical conductivity *vs* photon energy is shown in Fig. 4b. It decreases at higher photon energy. The opto-electrical conductivity decreases with increasing the caffeine content in $MAPbI_3$ from 0.5 to 1.0 wt% before it increases thereafter. With moderate caffeine content (0.5 to 1.0 wt%), it passivates defects and improves charge carrier mobility. When the caffeine content is increased further, the molecular interactions between caffeine and the absorbing perovskite could begin to disrupt the structural uniformity, leading to a reduction in charge carrier mobility and subsequent introduction of barriers or scattering centers, slowing down carrier transport.

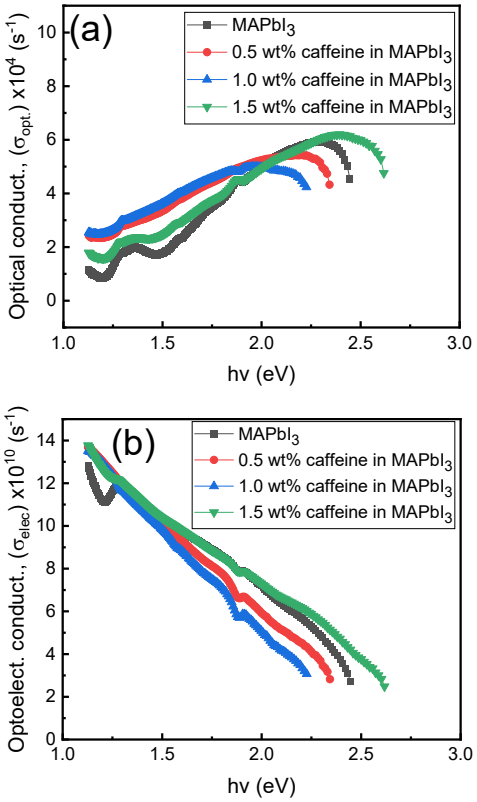

Fig. 4. Optical (a) and optoelectronic (b) conductivities with photon energy of the studied samples.

3.1.4. Real and imaginary dielectric constants

Dielectric constant is one of the fundamental properties of semiconducting materials. The dielectric constant can either be real (ε_r) or imaginary (ε_i). ε_r is the measure of material to slow down light speed, while ε_i is the measure of how much a material can absorb photons from an electric field as a result of dipole moment [5].

Figs. 5a and 5b depict the relationship of ε_r and ε_i with photon energy. ε_r decreases with increasing the caffeine content in $MAPbI_3$ from 0.5 to 1.0 wt%, but sharply increases with 1.5 wt% caffeine content. The imaginary dielectric constant increased towards higher photon energy (lower wavelength) for 0.5 and 1.0 wt%, reaching a maximum at 1.8 eV, and then decreased in the visible region. The reason for high ε_i and low ε_r at 0.5 and 1.0 wt% of caffeine is attributed to the higher absorption coefficient demonstrated by the as-prepared films, as shown in Fig. 3a.

3.1.5. Band gap energy

The energy band gap E_g (Tauc plot) of the pure $MAPbI_3$ and all samples with caffeine are shown in Fig. 6. The determination of the band gap value was achieved by simply extrapolating the linear part of the graph plotted for $(\alpha h\nu)^2$ *vs* $h\nu$, where α is the absorption coefficient, h is the Planck constant, and ν is the light frequency. It can be seen that when 0.5 wt% of caffeine was added to $MAPbI_3$, E_g was increased to 1.57 eV, which can be attributed to lower electronegativity, weaker covalent bonding strength among caffeine molecules compared to Pb in $MAPbI_3$. At 1.0 wt% of caffeine in $MAPbI_3$, E_g reduced to 1.40 eV, which is ascribed to stronger electronegativity [38]. Caffeine has previously reduced the band gap of $MAPbI_3$ [33]. At 1.5 wt% of caffeine in $MAPbI_3$, E_g further increased to 1.60 eV. The increase can be attributed to a decrease in grain size, resulting in larger grain boundaries which subsequently create vacancies, resulting in defects that spread on the surface, resulting in reduced E_g.

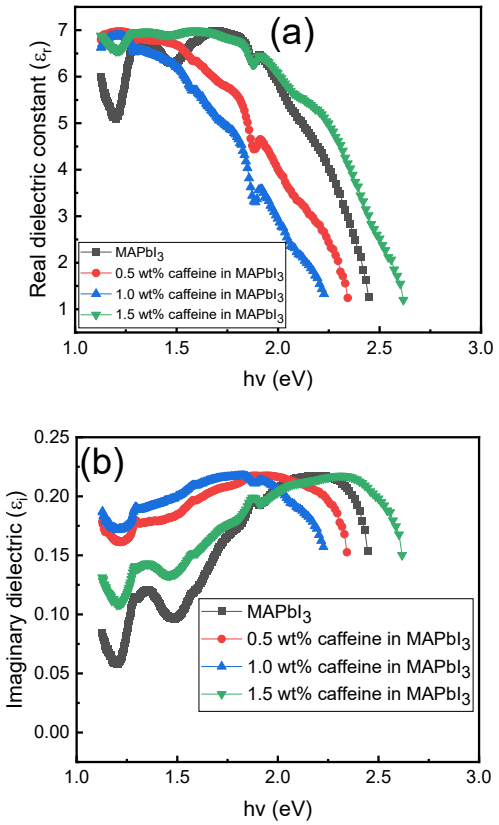

Fig. 5. Real (a) and imaginary (b) parts of the dielectric constant with photon energy for the studied samples.

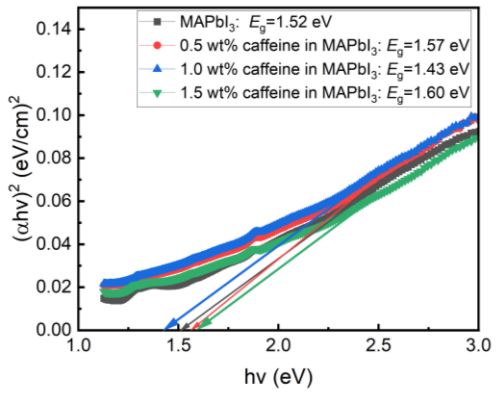

Fig. 6. Tauc plot for pure MAPbI3 and MAPbI3 with 0.5, 1.0, and 1.5 wt% of caffeine.

3.2. Microstructural properties

To confirm the formation of methyl ammonium lead triiodide perovskite, and $MAPbI_3$ with different wt% of caffeine, XRD measurements were carried out. Fig. 7 shows the XRD patterns of pure $MAPbI_3$ and $MAPbI_3$ with caffeine. For both $MAPbI_3$ film and $MAPbI_3$ films modified with caffeine, the diffraction peak at $2\theta = 11.98°$ is assigned to the (001) planes in hexagonal PbI_2. The strong peak at 13.37° and other peaks at 19.19°, 23.74°, 24.78°, 27.56°, 31.01°, 34.09°, 39.66°, 34.09°, 39.66°, 42.28°, 49.38°, and 51.61° with orientations (110), (200), (112), (022), (220), (310), (132), (141), (116), (404), and (226) confirmed the complete formation of $MAPbI_3$ perovskite film as well as $MAPbI_3$ with caffeine. A preferred growth orientation along (110) was observed in the XRD patterns of $MAPbI_3$ and $MAPbI_3$ with caffeine, though other minor peaks were observed, too. These peaks correspond to the pure tetragonal (β) phase of $MAPbI_3$ perovskite, which agrees with results in [39–42]. The intensity of the dominant peak at (110) for the caffeine-modified $MAPbI_3$ is higher than that of pure $MAPbI_3$. This indicates that the caffeine-modified film grew faster along (110) due to consuming the dispersedly oriented neighboring crystals [43]. The superior crystallinity of the caffeine-modified perovskite might be due to the suppression of ion migration.

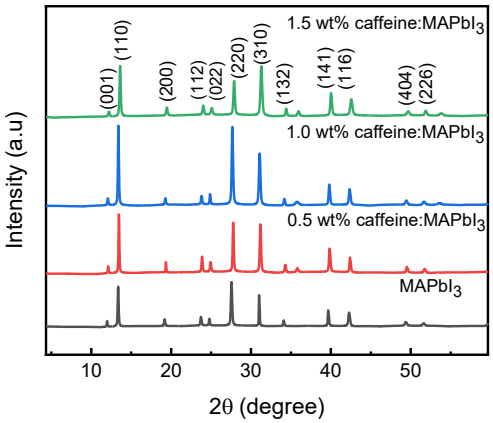

Fig. 7. XRD patterns of pure $MAPbI_3$ and $MAPbI_3$ with caffeine.

The parameters of the as-prepared films were calculated using Eqs. (4)–(6). The average crystallite size D was obtained from the Debye–Scherrer method, Eq. (4). The lattice strain (ε) and stacking fault (SF) were estimated using Eqs. (5) and (6), respectively [35, 44]:

$$D = \frac{0.9\lambda}{\beta \cos\theta}, \tag{4}$$

$$\varepsilon = \beta/4 \tan\theta, \tag{5}$$

$$SF = \left[\frac{2\pi^2}{45(3\tan\theta)^{1/2}}\right]\beta, \tag{6}$$

where λ represents the wavelength of the X-ray (λ = 0.1541 nm), β stands for full width at half maximum (FWHM) in radian, and θ represents the diffraction angle in degrees.

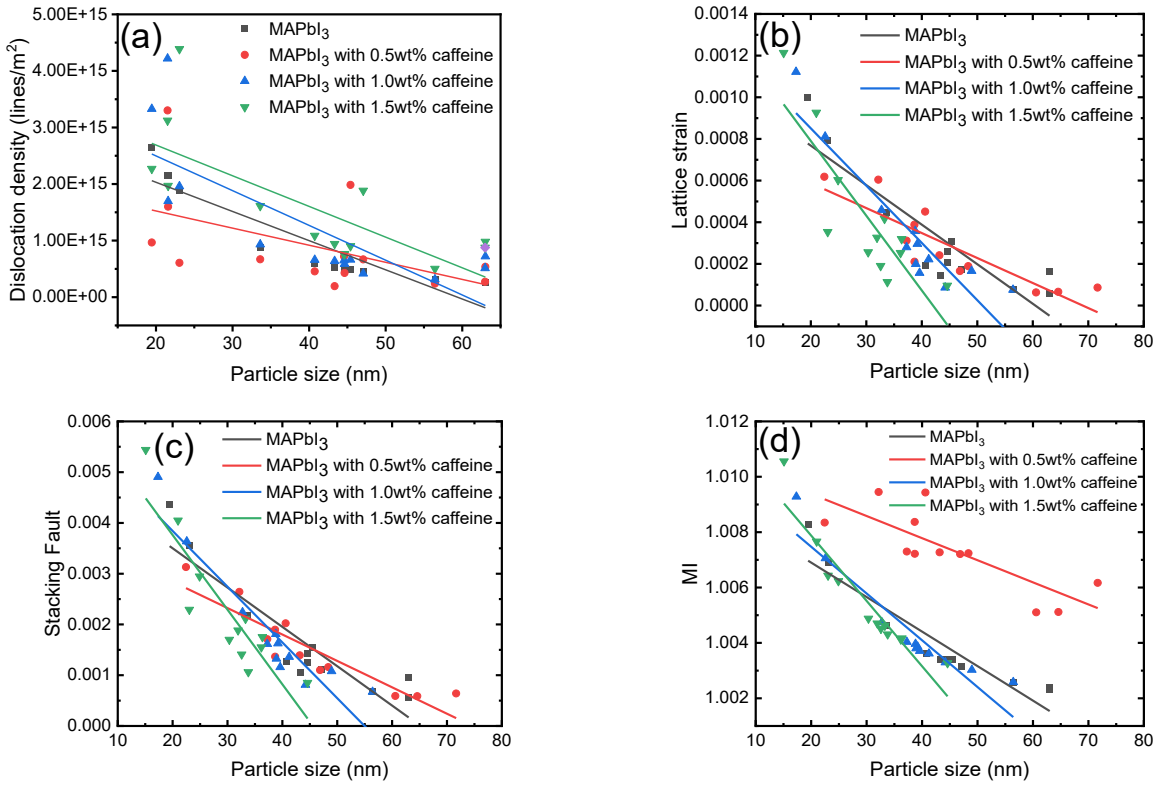

Fig. 8. Relationship between (a) dislocation density, (b) lattice strain, (c) stacking fault, (d) morphological index and particle size.

The crystallite size increases with increasing the amount of caffeine added. This is due to the increase in the overall film thickness with the addition of caffeine at the perovskite surface. The amount of caffeine added increased the size of the crystallites, as shown in Fig. 8a. This increase can be supported by the decreasing values of dislocation density and the lattice strain (see Figs. 8a and 8b), which indicates a more homogeneous film formation [35]. Table 1 shows the slope of these straight lines, and the intercept gives the average particle size. The dislocation density of all samples is indirectly proportional to the particle size. An increase in particle size results in a decrease in dislocation density. Strain hardening causes a decrease in dislocation density and variation in crystallite size. The stacking fault also has an inverse relationship with the crystallite size (see Fig. 8c). The corresponding decrease in the stacking fault affirmed our assertion on good crystal film formation. Also, the morphological index is indirectly proportional to the particle size, which confirms the uniformity of the prepared films (see Fig. 8d). The XRD results confirmed why the absorption coefficient, extinction coefficient, and optical conductivity improved at moderate caffeine contents and established why the bandgap narrowed at 1.0 wt%, and served as the structural validation of the optical improvements.

Table 1. The slope of straight line (intrinsic strain) and intercept (crystal size) from dislocation density *vs* particle size curve.

Sample	Intercept	Slope
$MAPbI_3$	3.06388E15	–5.16099E13
$MAPbI_3$ with 0.5wt% caffeine	2.12885E15	–3.02563E13
$MAPbI_3$ with 1.0wt% caffeine	3.72846E15	–6.15021E13
$MAPbI_3$ with 1.5wt% caffeine	3.77549E15	–5.42862E13

Table 2. The values of the intrinsic strain and average particle size.

Sample	Intercept	Slope
$MAPbI_3$	7.50675E–4	4.58426E–4
$MAPbI_3$ with 0.5wt% caffeine	8.52742E–4	5.09436E–4
$MAPbI_3$ with 1.0wt% caffeine	8.11071E–4	5.37395E–4
$MAPbI_3$ with 1.5wt% caffeine	2.60000E–3	6.23294E–4

Table 3. *J–V* characteristics of the studied devices.

Device	PCE (%)	*FF* (%)	J_{sc} (mA/cm^2)	V_{oc} (V)
A	6.157	0.639	10.132	0.951
B	12.313	0.642	20.183	0.951
C	14.072	0.640	23.083	0.953
D	10.554	0.639	17.360	0.951

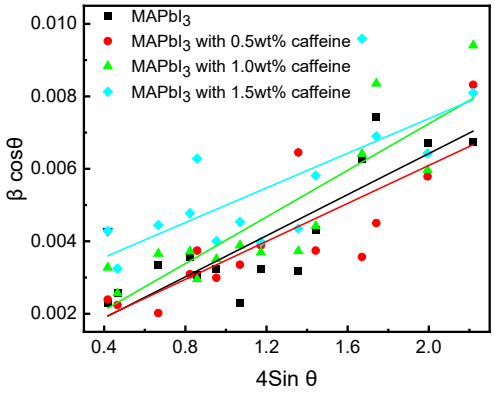

Fig. 9. Williamson–Hall plot for the studied $MAPbI_3$ samples.

Further analysis using the Williamson–Hall method is depicted in Fig. 9 and Table 2. The analysis using the Williamson–Hall curve is necessary since the Scherrer formula only focuses on the effect of crystallite size on the XRD peak broadening and does not account for the microstructural properties of the lattice, *i.e.,* the intrinsic strain, due to defects, grain boundaries, triple junction and stacking faults [5, 45, 46]. In the plot of βcosθ against 4sinθ, the slope shows the values of the intrinsic strain, while the intercept gives the average particle size of the films. As the amount of caffeine increases, the gradient of the plot also increases.

3.3. Morphological investigation of the studied $MAPbI_3$ samples

Fig. 10 shows the surface morphology of pure $MAPbI_3$ and $MAPbI_3$ with caffeine. It can be seen that a large amount of perovskite nanocrystals is dispersed on the surface with a morphology that is tetragonal in shape. Figs. 10b–10d show the morphologies of the films with different amounts of caffeine. The particle size and surface morphology of the caffeine-modified films are larger compared to the pure perovskite, which has already been

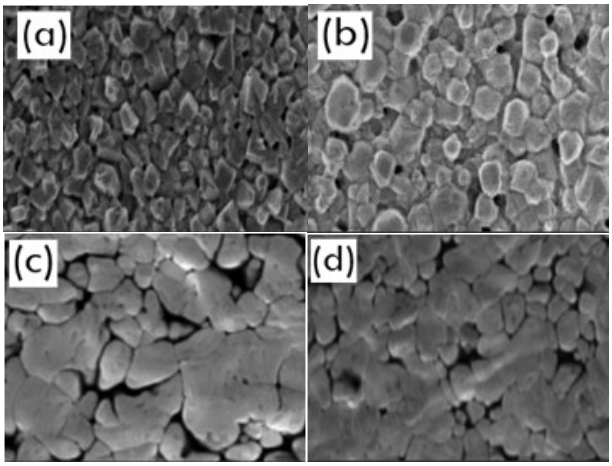

Fig. 10. SEM patterns for (a) pure $MAPbI_3$, (b) $MAPbI_3$ with 0.5 wt% of caffeine, (c) $MAPbI_3$ with 1.0 wt% of caffeine, and (d) $MAPbI_3$ with 1.5 wt% of caffeine.

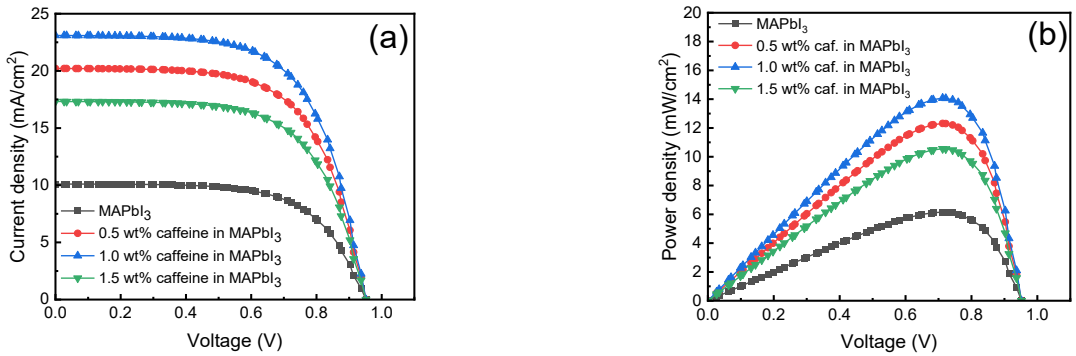

Fig. 11. (a) *J–V* curves and (b) *P–V* curves for the studied $MAPbI_3$ samples.

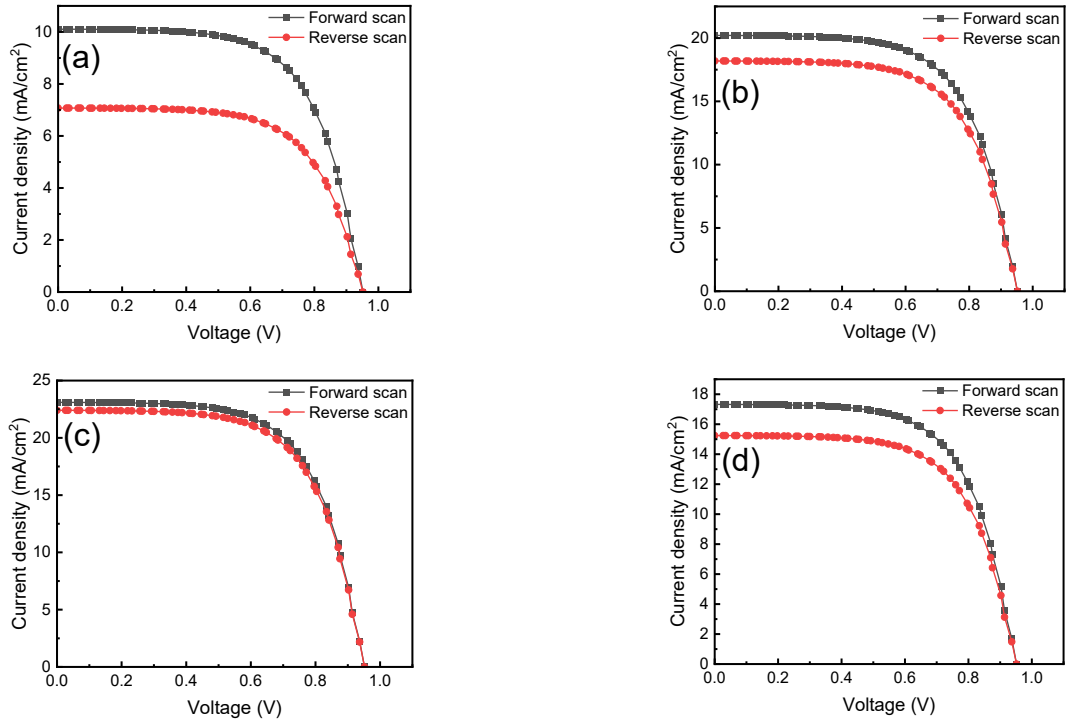

Fig. 12. The *J–V* hysteresis test for (a) pure $MAPbI_3$, (b) $MAPbI_3$ with 0.5 wt% of caffeine, (c) $MAPbI_3$ with 1.0 wt% of caffeine, and (d) $MAPbI_3$ with 1.5 wt% of caffeine.

confirmed by XRD. It was depicted from both surfaces that some PbI_2 grains are available due to incomplete reaction, which can be further confirmed from the (001) in XRD. The surface morphology of $MAPbI_3$ modified with various caffeine contents is rougher compared to pure $MAPbI_3$ perovskite. As a result, the grain of the latter is compact and smooth with better surface coverage in the latter than in the former. The increase in the particle size agrees with XRD results, which also leads to rougher morphology at higher caffeine content.

3.4. Photovoltaic study

The performances of the fabricated solar cells were obtained under 100 mW/cm^2 illumination. Fig. 11a displays the current-voltage (*J–V*) properties of the device with pure $MAPbI_3$, and 0.5, 1.0, and 1.5 wt% of caffeine in the $MAPbI_3$ absorber. The devices are summarized using the following four metric parameters. PCE, which is the overall efficiency of a solar cell, represents the percentage of incident light power converted into usable electrical energy. FF, which is the measure of the squareness of the *J–V* curve, indicating the quality of charge transport and internal resistive losses in the device. J_{sc}, which is the maximum photocurrent density generated under illumination when the external voltage is zero, reflecting light absorption and charge collection efficiency. V_{oc} is the maximum voltage produced under illumination when no current flows, determined by the difference in quasi-Fermi levels and influenced by recombination losses. The reference device without caffeine shows PCE of 6.157%, FF of 0.639, J_{sc} of 10.132 mA/cm^2, and V_{oc} of 0.951 V. When 0.5 wt% of caffeine was incorporated into device, the metric parameters was improved: PCE = 12.313%, FF = 0.642, J_{sc} = 20.183 mA/cm^2, and V_{oc} = 0.951 V. Further increase on the caffeine content to 1.0 wt% also improved

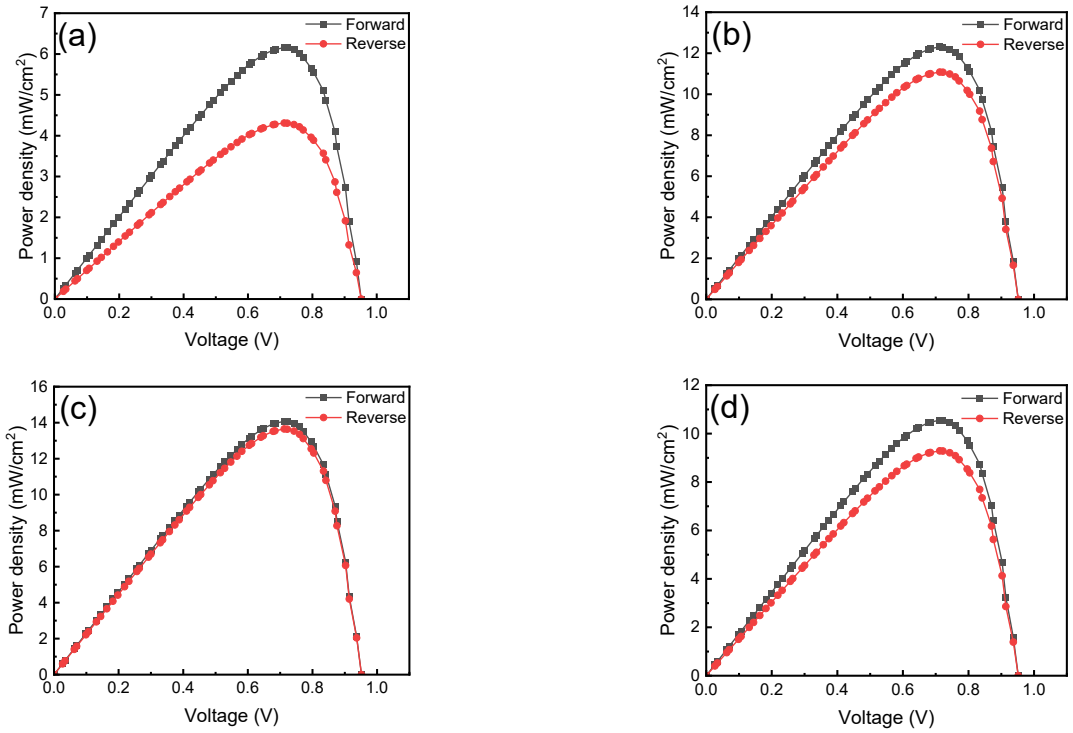

Fig. 13. The power density for (a) pure MAPbI3, (b) MAPbI3 with 0.5 wt% of caffeine, (c) MAPbI3 with 1.0 wt% of caffeine, and (d) MAPbI3 with 1.5 wt% of caffeine.

Table 4. Comparison of PV parameters with those published in the literature.

Additives	Device	PCE	FF	J_{sc}	V_{oc}	Ref.
Ethoxyethanol	ITO/ZnO/perovskite/spiro-OMeTAD/MoOx/Ag	13.20	0.54	21.10	1.07	[47]
Fluorine	ITO/PEDOT:PSS/$MAPbI_3$/PCPM/Al	13.00	0.78	18.50	0.98	[48]
Ammonium acetate	FTO/TiO_2/$MAPbI_3$/Carbon	13.88	0.59	24.35	0.98	[49]
Zinc acetate	FTO/TiO_2/$MAPbI_3$/Carbon	12.30	0.59	22.60	0.92	[49]
Caffeine	ITO/TiO_2/$MAPbI_3$/CuI/Elcocarb	14.072	0.640	23.083	0.953	[This work]

PCE to 14.072%, J_{sc} to 23.083 mA/cm^2 and V_{oc} to 0.953 V. Contrary to the improvement, there was a decrease in FF for 1.0 wt% caffeine-modified device. Whereas the photovoltaic performance decreases with further increase in caffeine content to 1.5 wt%. As shown in Table 3, the best device was with 1.0 wt% of caffeine in the perovskite absorber. The improved performance caused by caffeine can be attributed to a higher concentration of charge carriers with a long diffusion length [35]. The enhanced V_{oc} and FF are ascribed to the decrease in non-radiative recombination and crystal defects due to the passivation effect [35].

From Table 3, it can be concluded that the caffeine-modified devices showed improved PV performance compared to the device lacking caffeine. This outstanding performance can be attributed to the presence of the functional groups (*i.e.*, C=O, CH_3, C=C, and –C=N) in caffeine, which created strong bonding interaction with Pb^{2+} ions in $MAPbI_3$, and resulted in the growth of a high-quality nanocrystalline absorbing film [35, 43]. Additionally, the absolute coverage of caffeine in the $MAPbI_3$ absorber effectively resulted in efficient transport of charge carriers, while mitigating e–h recombination at the device interfaces. The power density against the voltage is shown in Fig. 11b. The compared parameters of various devices are summarized in Table 4.

The *J–V* hysteresis was also evaluated, and the plot is shown in Figs. 12a–12d. The effect of hysteresis gives rise to disparity in the current-voltage measurement, and it becomes difficult to estimate the actual PCE of a PSC device. The major cause of hysteresis is not fully understood, but some possible suggestions for the cause of hysteresis are attributed to ion migration, charge trapping, and detrapping as well as accumulation [5]. To evaluate the hysteresis, the devices were tested both at forward and reverse scan. The *J–V* hysteresis between the reverse and forward scan directions was reduced with the addition of caffeine. The average PCE was improved from 5.234 to 11.698% at 0.5 wt% of caffeine in perovskite, from 5.234 to 13.861% at 1.0 wt% of caffeine

Table 5. PV metrics of the forward and reverse scan for reference and caffeine-modified devices.

Device	Scan	PCE (%)	*FF* (%)	J_{sc} (mA/cm^2)	V_{oc} (V)	HI
A	F R	6.157 4.310	0.639 0.639	10.132 7.087	0.951 0.951	0.3000
B	F R	12.313 11.082	0.642 0.639	20.183 18.234	0.951 0.951	0.0902
C	F R	14.072 13.650	0.640 0.639	23.083 22.482	0.953 0.953	0.0300
D	F R	10.554 9.288	0.639 0.642	17.360 15.215	0.951 0.951	0.1200

in perovskite, and from 5.234 to 9.921% at 1.5 wt% of caffeine in perovskite. The hysteresis index (HI) for the *J–V* curves was calculated from Eq. (7) [5]:

$$\mathrm{HI} = \frac{\mathrm{PCE_{FS}} - \mathrm{PCE_{RS}}}{\mathrm{PCE_{FS}}}, \qquad (7)$$

where $\mathrm{PCE_{FS}}$ is the forward voltage scan efficiency, and $\mathrm{PCE_{RS}}$ is the reverse voltage scan efficiency. When a device has HI of zero, it means it has no hysteresis, while the higher HI values imply significant hysteresis [50]. The devices made of various amounts of caffeine show reduced hysteresis than the pristine device, as shown in Table 5. The *P–V* plots for the various devices are depicted in Fig. 13.

The device lacking caffeine shows forward and reverse scans PCEs of 6.157% and 4.310%, respectively, producing an average PCE of 5.234%. This shows an HI of 0.3000. The device with 0.5 wt% of caffeine in $MAPbI_3$ shows PCE of 12.313%, FF of 0.642, J_{sc} of 20.183 mA/cm^2, and V_{oc} of 0.951 V during the forward scan, while PCE of 11.082%, FF of 0.639, J_{sc} of 18.234 mA/cm^2, and V_{oc} of 0.951 V are obtained during the reverse scan. The device with 1.0 wt% caffeine gave PCE of 14.072% during forward scan and 13.650% PCE during the reverse scan. The device with 1.5 wt% shows 10.554% and 9.288% PCEs during the forward and reverse scan. The power density against voltage for the forward and reverse scan is shown in Fig. 13a–13d. The plot that compares various devices with corresponding HI is shown in Fig. 14.

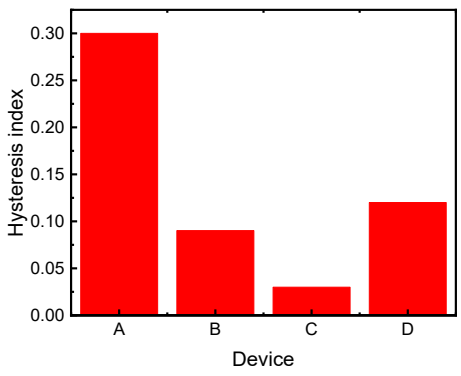

Fig. 14. Hysteresis index for various devices.

4. Conclusion

In this study, perovskite solar cells based on $MAPbI_3$ with various contents of caffeine (0.5, 1.0, and 1.5 wt%) were fabricated. The effect of the introduced caffeine was probed using XRD, UV-vis, and SEM. PV performances were evaluated under 100 mW/cm^2 illumination. From the results of the study, the following findings were reached when caffeine was incorporated into the perovskite film:

(1) Addition of caffeine facilitated the absorption of light and the growth of high-quality crystal film.
(2) Incorporating caffeine into $MAPbI_3$ resulted in improved photovoltaic parameters (V_{oc}, J_{sc}, FF, and PCE). In particular, the best device was obtained with 1.0 wt% of caffeine in $MAPbI_3$, which gave PCE of 14.072%.
(3) Introducing caffeine in the $MAPbI_3$ perovskite greatly increases the electron-hole charge carriers.
(4) The devices with caffeine molecules experienced less hysteresis, with the 1.0 wt% based device having the least hysteresis index of 0.0300.

This research demonstrates that caffeine can passivate $MAPbI_3$ crystallites and transport carriers over short distances, which can cause high-quality devices with potential for industry scalability.

Acknowledgement

The authors appreciate the financial support from the Tertiary Education Trust Fund through the internally based research of Federal University of Health Sciences, Otukpo (FUHSO), under grant number 2023/FX302-IBR.

References

1. Holechek J.L., Geli H.M.E., Sawalhah M.N., Valdez R. A global assessment: Can renewable energy replace fossil fuels by 2050? *Sustainability.* 2022. **14**. P. 4792. https://doi.org/10.3390/su14084792.
2. Chanchangi Y.N., Adu F., Ghosh A. *et al*. Nigeria's energy review: Focusing on solar energy potential and penetration. *Environ. Dev. Sustain*. 2023. **25**. P. 5755–5796. https://doi.org/10.1007/s10668-022-02308-4.
3. Adeola A.O., Akingboye A.S., Ore O.T. *et al.* Crude oil exploration in Africa: socio-economic implications, environmental impacts, and mitigation strategies. *Environ. Syst. Decis*. 2022. **42**. P. 26–50. https://doi.org/10.1007/s10669-021-09827-x.

4. Danladi E., Egbugha A.C., Obasi R.C. *et al.* Defect and doping concentration study with series and shunt resistance influence on graphene modified perovskite solar cell: A numerical investigation in SCAPS-1D framework. *J. Indian Chem. Soc.* 2023. **100**. P. 101001. https://doi.org/10.1016/j.jics.2023.101001.
5. Danladi E., Ichoja A., Onoja E.D. *et al.* Broad-band-enhanced and minimal hysteresis perovskite solar cells with interfacial coating of biogenic plasmonic light trapping silver nanoparticles. *Mater. Res. Innov.* 2023. **27**. P. 521–536. https://doi.org/10.1080/14328917.2023.2204585.
6. Zhang J., Li C., Zhu M. *et al.* Stable and environmentally friendly perovskite solar cells induced by grain boundary engineering with self-assembled hydrogen-bonded porous frameworks. *Nano Energy*. 2023. **108**. P. 108217. https://doi.org/10.1016/j.nanoen.2023.108217.
7. Ai B., Fan Z., Wong Z.J. Plasmonic perovskite solar cells, light emitters and sensors. *Microsyst. Nanoeng*. 2022. **8**. P. 5. https://doi.org/10.1038/s41378-021-00334-2.
8. Al-Ezzi A.S., Ansari M.N.M. Photovoltaic solar cells: A review. *Appl. Syst. Innov*. 2022. **5**. P. 67. https://doi.org/10.3390/asi5040067.
9. Hossain M.K., Toki G.F.I., Alam I. *et al*. Numerical simulation and optimization of a $CsPbI_3$-based perovskite solar cell to enhance the power conversion efficiency. *New J. Chem.* 2023. **47**. P. 4801–4817. https://doi.org/10.1039/D2NJ06206B.
10. Durodola O.M., Ugwu C., Danladi E. Highly efficient lead-free perovskite solar cell based on magnesium doped copper delafossite hole transport layer: A SCAPS-1D framework prospect. *Emerg. Mater*. 2023. **6**. P. 1665–1684. https://doi.org/10.1007/s42247-023-00542-8.
11. Sumona F.B., Kashif M., Danladi E. *et al*. Optimization of perovskite-$KSnI_3$ solar cell by using different hole and electron transport layers: A numerical SCAPS-1D simulation. *Energy Fuels*. 2023. **37**. P. 19207–19219. https://doi.org/10.1021/acs.energyfuels.3c02397.
12. Nyiekaa E.A., Aika T.A., Danladi E. *et al*. Simulation and optimization of 30.17% high performance N-type TCO-free inverted perovskite solar cell using inorganic transport materials. *Sci. Rep*. 2024. **14**. P. 12024. https://doi.org/10.1038/s41598-024-62882-7.
13. Nyiekaa E.A., Aika T.A., Orukpe P.E. *et al*. Development on inverted perovskite solar cells: A review. *Heliyon*. 2024. **10**. P. e24689. https://doi.org/10.1016/j.heliyon.2024.e24689.
14. Kim D.I., Lee J.W., Jeong R.H., Boo H.-H. A high-efficiency and stable perovskite solar cell fabricated in ambient air using a polyaniline passivation layer. *Sci. Rep*. 2022. **12**. P. 697. https://doi.org/10.1038/s41598-021-04547-3.
15. Kojima A., Teshima K., Shirai Y., Miyasaka T. Organometal halide perovskites as visible-light sensitizers for photovoltaic cells. *J. Am. Chem. Soc.* 2009. **131**. P. 6050–6051. https://doi.org/10.1021/ja809598r.
16. Qu Z., Ma F., Zhao Y. *et al*. Updated progresses in perovskite solar cells. *Chin. Phys. Lett.* 2021. **38**. P. 107801. https://doi.org/10.1088/0256-307X/38/10/107801.
17. Danladi E., Onimisi M.Y.*et al*. 9.05% HTM free perovskite solar cell with negli-gible hysteresis by introducing silver nanoparticles encapsulated with P_4VP polymer. *SN Appl. Sci.* 2020. **2**. P. 1769. https://doi.org/10.1007/s42452-020-03597-y.
18. Chowdhury T.A., Zafar M.A.B., Islam M.S. *et al*. Stability of perovskite solar cells: Issues and prospects. *RSC Adv*. 2023. **13**. P. 1787–1810. https://doi.org/10.1039/D2RA05903G.
19. Yang H., Li X., Guo X. *et al*. Enhancing the stability of perovskite solar cells through an iodine confining strategy. *ACS Energy Lett*. 2023. **8**. P. 3793–3799. https://doi.org/10.1021/acsenergylett.3c01330.
20. Jeon N.J., Na H., Jung E.H. *et al*. A fluorene-terminated hole-transporting material for highly efficient and stable perovskite solar cells. *Nat. Energy*. 2018. **3**. P. 682–689. https://doi.org/10.1038/s41560-018-0200-6.
21. Abdi-Jalebi M., Andaji-Garmaroudi Z., Cacovich S. *et al*. Maximizing and stabilizing luminescence from halide perovskites with potassium passivation. *Nature*. 2018. **555**. P. 497–501. https://doi.org/10.1038/nature25989.
22. Jin S., Wei Y., Yang X. *et al*. Additive engineering induced perovskite crystal growth for high performance perovskite solar cells. *Org. Electron*. 2018. **63**. P. 207–215. https://doi.org/10.1016/j.orgel.2018.09.040.
23. Wang Z., Chen S., Gao X. PTB7 as additive in anti-solvent to enhance perovskite film surface crystallinity for solar cells with efficiency over 21%. *Appl. Surf. Sci*. 2022. **575**. P. 151737. https://doi.org/10.1016/j.apsusc.2021.151737.
24. Bi D., Yi C., Luo J. *et al*. Polymer-templated nucleation and crystal growth of perovskite films for solar cells with efficiency greater than 21%. *Nat. Energy*. 2016. **1**. P. 1–8. https://doi.org/10.1038/nenergy.2016.142.
25. Guo X., Ma J., Lei H. *et al*. Enhanced performance of perovskite solar cells via anti-solvent nonfullerene Lewis base IT-4F induced trap-passivation. *J. Mater. Chem. A*. 2018. **6**. 5919–5925. https://doi.org/10.1039/C8TA00583D.
26. Wang F., Yang M., Yang S. *et al*. Iodine-assisted anti-solvent engineering for stable perovskite solar cells with efficiency >21.3%. *Nano Energy*. 2020. **67**. P. 104224. https://doi.org/10.1016/j.nanoen.2019.104224.
27. Niu T., Lu J., Munir R. *et al*. Stable high-performance perovskite solar cells via grain boundary passivation. *Adv. Mater.* 2018. **30**. P. 1706576. https://doi.org/10.1002/adma.201706576.
28. Kumar P., Vahidzadeh E., Thakur U.K. *et al.* C_3N_5: A low bandgap semiconductor containing an azo-linked carbon nitride framework for photocatalytic, photovoltaic and adsorbent applications. *J. Am.*

Chem. Soc. 2019. **141**. P. 5415–5436. https://doi.org/10.1021/jacs.9b00144.
29. Li Z., Feng J., Cao J. *et al*. New carbon nitride C_3N_3 additive for improving cationic defects of perovskite solar cells. *Energy Environ. Mater*. 2023. **6**. P. e12283. https://doi.org/10.1021/jacs.9b00144.
30. Kim D.W., Choi J., Byun J. *et al*. Monodisperse carbon nitride nanosheets as multifunctional additives for efficient and durable perovskite solar cells. *ACS Appl. Mater. Interfaces.* 2021. **13**. P. 61215–61226. https://doi.org/10.1021/acsami.1c19587.
31. Ho C.M., Wu M.C., Chen S.H. *et al*. High-performance stable perovskite solar cell via defect passivation with constructing tunable graphitic carbon nitride. *RRL Solar.* 2021. **5**. P. 2100257. https://doi.org/10.1002/solr.202170084.
32. Zhao X., Wang S., Shan X. *et al*. Fabrications of halide perovskite single-crystal slices and their applications in solar cells, photodetectors, and LEDs. *Cryst. Growth Des*. 2021. **21**. P. 5983–5997. https://doi.org/10.1021/acs.cgd.1c00548.
33. Dhanabal R., Kasinathan D., Mahalingam A. *et al*. Caffeine additive based nanoarchitectonics of methylammonium lead iodide ($MAPbI_3$) perovskite solar cell device: Investigations on charge carrier properties using AC impedance spectroscopy. *J. Mater. Sci.: Mater. Electron*. 2023. **34**. P. 2205. https://doi.org/10.1007/s10854-023-11569-2.
34. Kure N., Onimisi M.Y., Ali H. *et al*. A caffeine doped perovskite solar cells without hole transporting material. *Academy J. Sci. Eng*. 2024. **18**. P. 108–117.
35. Jubu P.R., Bem T.T., Ndeze U.I. *et al*. Optical and optoelectronic properties of gallium oxide films fabricated by the chemical vapour deposition method. *Phys. B Condens. Matter*. 2024. **678**. P. 415763. https://doi.org/10.1016/j.physb.2024.415763.
36. Hassanien A.M., Atta A.A., El-Nahass M.M. *et al*. Effect of annealing temperature on structural and optical properties of gallium oxide thin films deposited by RF-sputtering. *Opt. Quant. Electron*. 2020. **52**. P. 194. https://doi.org/10.1007/s11082-020-02306-8.
37. Tasiu J., Onimisi M. Y., Yusuf A.S. *et al*. Effect of biosynthesized silver nanoparticles on the optical, structural, and morphological properties of TiO_2 nanocrystals. *East Eur. J. Phys.* 2024. **1**. P. 315–321. https://doi.org/10.26565/2312-4334-2024-1-28.
38. Zhou Y., Chen J., Bark O. *et al*. Metal-doped lead halide perovskites: Synthesis, properties, and optoelectronic applications. *Chem. Mater.* 2018. **30**. P. 6589–6613. https://doi.org/10.1021/acs.chemmater.8b02989.
39. Chen L., Lee K., Wu W. *et al*. Effect of different $CH_3NH_3PbI_3$ morphologies on photovoltaic properties of perovskite solar cells. *Nanoscale Res. Lett*. 2018. **13**. P. 140. https://doi.org/10.1186/s11671-018-2556-8.
40. Basumatary P., Agarwal P. Photocurrent transient measurements in $MAPbI_3$ thin films. *J. Mater. Sci.: Mater. Electron*. 2020. **31**. P. 10047–10054. https://doi.org/10.1007/s10854-020-03549-7.
41. Guo X., McCleese C., Kolodziej C. *et al*. Identification and characterization of the intermediate phase in hybrid organic–inorganic $MAPbI_3$ perovskite. *Dalton Trans*. 2016. **45**. P. 3806–3813. https://doi.org/10.1039/C5DT04420K.
42. Zhou Y., Yang M., Vasiliev A.L. *et al*. Growth control of compact $CH_3NH_3PbI_3$ thin films *via* enhanced solid-state precursor reaction for efficient planar perovskite solar cells. *J. Mater. Chem. A*. 2015. **3**. P. 9249–9256. https://doi.org/10.1039/C4TA07036D.
43. Wang R., Xue J., Meng L. *et al*. Caffeine improves the performance and thermal stability of perovskite solar cells. *Joule*. 2019. **3**. P. 1464–1477. https://doi.org/10.1016/j.joule.2019.04.005.
44. Jubu P.R., Danladi E., Chahul H.F. *et al*. Photoanodic properties of In/β-Ga_2O_3 nanostructures fabricated under hydrogen reducing ambient by the vapour-phase growth method. *Opt. Mater.* 2023. **145**. P. 114424. https://doi.org/10.1016/j.optmat.2023.114424.
45. Hall W.H. X-ray line broadening in metals. *Proc. Phys. Soc. A*. 1949. **62**. P. 741–743. https://doi.org/10.1088/0370-1298/62/11/110.
46. Nath D., Singh F., Das R. X-ray diffraction analysis by Williamson-Hall, Halder-Wagner and size-strain plot methods of CdSe nanoparticles – a comparative study. *Mater. Chem. Phys*. 2020. **239**. P. 122021. https://doi.org/10.1016/j.matchemphys.2019.122021.
47. Ugur E., Sheikh A.D., Munir R. *et al*. Improved morphology and efficiency of *n–i–p* planar perovskite solar cells by processing with glycol ether additives. *ACS Energy Lett*. 2017. **2**. P. 1960–1968. https://doi.org/10.1021/acsenergylett.7b00526.
48. Kim G., Jang H., Yoon Y. *et al*. Fluorine functionalized graphene nano platelets for highly stable inverted perovskite solar cells. *Nano Lett*. 2017. **17**. P. 6385–6390. https://doi.org/10.1021/acs.nanolett.7b03225.
49. Zhang Z., Fan W., Wei X. *et al*. Promoted performance of carbon based perovskite solar cells by environmentally friendly additives of CH_3COONH_4 and $Zn(CH_3COO)_2$. *J. Alloys Compd*. 2019. **802**. P. 694–703. https://doi.org/10.1016/j.jallcom.2019.06.161.
50. Mohammed M.K.A., Jabir M.S., Abdulzahraa H.G. *et al*. Introduction of cadmium chloride additive to improve the performance and stability of perovskite solar cells. *RSC Adv.* 2022. **12**. P. 20461–20470. https://doi.org/10.1039/D2RA03776A.

Authors and CV

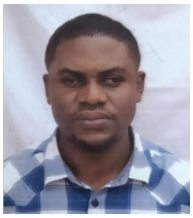

Matthew I. Amanyi obtained his M.Sc degree in Physics at the Nigerian Defence Academy in 2006. He is currently a faculty member in the Department of Physics at the Federal University of Health Sciences, Otukpo, Nigeria, and a PhD student at the Nasarawa State University, Nigeria.
E-mail: matthew.amanyi@fuhso.edu.ng,
https://orcid.org/0000-0003-1087-4775

Eli Danladi received his PhD degree from the Nigerian Defence Academy in 2020. His research interests are in materials science, device modeling, nanomaterials, and their applications in photovoltaic devices, batteries, and supercapacitors.
https://orcid.org/0000-0001-5109-4690

AbdulAzeez O. Salawu obtained his M.Sc degree in Physics from the Nigerian Defence Academy in 2017. He is currently a faculty member in the Department of Computer Science at Nile University of Nigeria, Abuja, and also a PhD student at the same University.
E-mail: zeezsalawu@gmail.com,
https://orcid.org/0000-0002-3159-8768

Alhaji I. Alhaji received his M.Sc degree in Physics from the Nigerian Defence Academy, Nigeria, in 2020. He is currently a staff member in the Department of Science Education at the Federal University Dutsin-Ma, Nigeria, where he is actively involved in research and teaching.
E-mail: rawayau85@gmail.com,
https://orcid.org/0009-0000-1702-4461

Kehinde A. Ogunmoye obtained his M.Sc. degree in Photonics from Friedrich Schiller Universität, Jena, Germany, in 2021. He is presently doing a second M.Sc degree in the Department of Physics and Astronomy, Appalachian State University, Boone, North Carolina, USA. His research interests include physics of surfaces and optics, hetero- and hybrid structures and devices (photoresistors, light-emitting structures etc.). http://orcid.org/0009-0003-0408-7035, e-mail: ogunmoyeka@appstate.edu

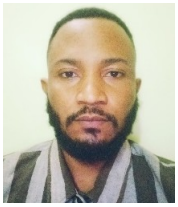

Onah E. Onah received his M.Sc degree in Physics from Federal University of Lafia, Nigeria, in 2025. He is currently a faculty member in the Department of Physics at the Federal University of Health Sciences, Otukpo, Nigeria, where he is actively involved in research. E-mail: onah.e.o@gmail.com,
http://orcid.org/0000-0002-7452-8364

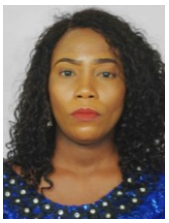

Mary T. Ekwu received her M.Sc. degree in Physics from the Nigerian Defence Academy in 2018. She is presently a faculty member in the Department of Physics, Air Force Institute of Technology, Kaduna, Nigeria, where she is actively involved in research and teaching. E-mail: tonghamary@gmail.com,
https://orcid.org/0009-0005-6154-4073

Authors' contributions

Amanyi M.I.: formal analysis, investigation, data curation, visualization, writing – original draft, writing – review & editing.
Danladi E.: conceptualization, methodology, validation, formal analysis, investigation, resources, data curation, writing – original draft.
Salawu A.O.: investigation, project administration.
Alhaji A.I.: investigation, resources.
Ogunmoye K.A.: investigation.
Onah O.E.: investigation, resources.
Ekwu M.T.: investigation, resources, validation, writing – review & editing.

Підвищена фотоелектрична продуктивність та мінімальний гістерезис перовскітних сонячних елементів з використанням модифікованого кофеїном світлозбирального матеріалу $MAPbI_3$

M.I. Amanyi, E. Danladi, A.O. Salawu, A.I. Alhaji, K.A. Ogunmoye, O.E. Onah, M.T. Ekwu

Анотація. Перовскітні сонячні елементи (PSCs) стали висхідною зіркою на горизонті фотоелектричної енергетики завдяки своїй економічній ефективності та простому процесу виготовлення. Незважаючи на їх перспективність, їх комерціалізація була ускладнена через низьку ефективність перетворення енергії (PCE) та гістерезис. У цій статті для виготовлення PSCs кофеїн був доданий до йодиду метиламонію свинцю ($MAPbI_3$) з різною масовою часткою (0,5, 1,0 та 1,5 мас.%). Було досліджено вплив кофеїну на поглинання світла, кристалічність, продуктивність пристрою та вольт-амперні характеристики (гістерезис). Було встановлено, що додавання кофеїну приводить до покращення поглинання, зменшення ширини забороненої зони та покращення кристалічності плівки. PSCs з молекулами кофеїну продемонстрували покращені метричні параметри (PCE, коефіцієнт заповнення FF, густина струму короткого замикання J_{sc} та напруга холостого ходу V_{oc}) порівняно з пристроєм без кофеїну. Зокрема, пристрій з 1,0 ваг.% кофеїну у $MAPbI_3$ демонструє найкращі показники з PCE = 14,072%, FF = 0,640, J_{sc} = 23,083 мА/см^2 та V_{oc} = 0,953 В. Розбіжність у вимірюваннях вольт-амперних характеристик для всіх пристроїв на основі кофеїну зменшилася. Зокрема, пристрій з 1,0 ваг.% кофеїну мав індекс гістерезису 0,0300. Пристрій без кофеїну продемонстрував PCE = 6.157%, FF = 63.9%, J_{sc} = 10.132 mA/cm^2, і V_{oc} = 0.951 V, і працював гірше, ніж всі пристрої з включеннями кофеїну. Підвищені характеристики перовскіту, модифікованого кофеїном, пов'язані зі зменшеними послідовним опором і концентрацією центрів безвипромінювальної рекомбінації, що привело до більш ефективного переносу заряду та збільшеного часу життя носіїв у шарі поглинача.

Ключові слова: перовскітні сонячні елементи, кофеїн, гістерезис, фотовольтаїка.